J Neurophysiol 102: 2131–2141, 2009.
First published July 22, 2009; doi:10.1152/jn.91319.2008.

On the Nature of the Intrinsic Connectivity of the Cat Motor Cortex: Evidence for a Recurrent Neural Network Topology

Charles Capaday,[1] Christian Ethier,[1] Laurent Brizzi,[1] Attila Sik,[2] Carl van Vreeswijk,[3] and Denis Gingras[4]

[1]*Brain and Movement Laboratory, Dept. of Electrical Engineering, Division of Biomedical Engineering, Danish Technical University, Lyngby, Denmark;* [2]*Cellular Neuroscience, Division of Neuroscience, School of Medicine, University of Birmingham, Vincent Drive, Edgbaston, Birmingham, United Kingdom;* [3]*Neurophysique et Physiologie du Système Moteur, Paris, France; and* [4]*Department of Electrical Engineering, Université de Sherbrooke, Sherbrooke, Quebec, Canada*

Submitted 15 December 2008; accepted in final form 15 July 2009

Capaday C, Ethier C, Brizzi L, Sik A, van Vreeswijk C, Gingras D. On the nature of the intrinsic connectivity of the cat motor cortex: evidence for a recurrent neural network topology. *J Neurophysiol* 102: 2131–2141, 2009. First published July 22, 2009; doi:10.1152/jn.91319.2008. The details and functional significance of the intrinsic horizontal connections between neurons in the motor cortex (MCx) remain to be clarified. To further elucidate the nature of this intracortical connectivity pattern, experiments were done on the MCx of three cats. The anterograde tracer biocytin was ejected iontophoretically in layers II, III, and V. Some 30–50 neurons within a radius of ~250 μm were thus stained. The functional output of the motor cortical point at which biocytin was injected, and of the surrounding points, was identified by microstimulation and electromyographic recordings. The axonal arborizations of the stained neurons were traced under camera lucida. The axon collaterals were extensive, reaching distances of ≤7 mm from the injection site. More importantly, the axonal branches were studded all along their course with boutons. The vast majority of boutons formed synaptic contacts on the target cells as identified by electron microscopy. The majority of these boutons made asymmetric (type I, excitatory) synapses mainly on dendritic spines. The bouton density decreased approximately monotonically with distance from the center of the injection. Cluster analysis, lagged covariance analysis, and eigenvalue decomposition showed the bouton distribution map to be unimodal. Superposition of the synaptic bouton distribution map and the motor output map revealed that motor cortical neurons don't make point-to-point connections but rather bind together the representations of a variety of muscles within a large neighborhood. This recurrent-network type connectivity strongly supports the hypothesis that the MCx controls the musculature in an integrated manner.

INTRODUCTION

The purpose of this study was to elucidate the nature of the intracortical connectivity of the cat motor cortex (MCx) by combined neuroanatomical and -physiological experiments. A detailed understanding of the connectivity pattern and how it is related to the motor output "map" should reveal further operational principles of motor cortical function (Capaday 2004). Horizontal connections within and between cortical areas have often been described as patchy in nature (e.g., Bosking et al. 1997; Buzas et al. 2006; Huntley and Jones 1991; Lund et al. 1993; Rockland and Lund 1982), implying selectivity in the pattern of connections and a universal organizing principle. However, Van Hooser et al. (2006) have cautioned against broad generalization of patchy connectivity as a universal organizing principle of cortical connectivity. For example, in the gray squirrel while long range horizontal connections exist within the primary visual cortex, they are neither patchy nor periodic as they are in primates and carnivores (Van Hooser et al. 2006).

In the process of examining the neuroanatomical material of our study on the intrinsic connections between motor cortical points controlling antagonistic muscles in the cat (Capaday et al. 1998), we were struck by the fact that most synaptic boutons appeared to be located along the axons (i.e., bouton en passant) rather than concentrated at terminal fields. Thus the horizontal axon collaterals of motor cortex neurons are studded with boutons all along their course without significant concentrations of boutons patches. This striking anatomical fact has seldom been reported and its potential significance for MCx function remains to be elucidated. The connections made by horizontal collaterals in the MCx have been suggested to be an anatomical substrate of inter-joint muscle synergies (Huntley and Jones 1991; Keller 1993). However, the details and functional significance of the connectivity pattern remain to be clarified. Huntley and Jones (1991), as well as Keller (1993), interpreted the pattern of connectivity as being point-to-point on the basis of an apparently patchy distribution of stained axon fragments. In this perspective, a cortical point controlling, for example, the wrist connects to a cortical point controlling the shoulder but not to points that may lay in between, such as the elbow. However, if synaptic boutons are present all along the axon collaterals, this implies that all neurons contacted along their lengthy course (≤7 mm) will be affected. The purpose of this study was therefore to relate the intrinsic connectivity of the cat MCx, defined as the spatial distribution of synaptic boutons, to the muscle representation map. To this end, we injected the anterograde tracer biocytin at an identified cortical point and determined the density of synaptic boutons across the motor cortex. This bouton density map was superimposed in register with the muscle representation map determined by microstimulation and electromyographic (EMG) recordings. This work was published as an abstract (Ethier et al. 2006b).

METHODS

The data reported herein were obtained from three male cats weighing 3.1, 4.4, and 4.6 kg, respectively. The study was approved by the local ethics committee and conformed to the procedures

Address for reprint requests and other correspondence: C. Capaday, Brain and Movement Laboratory, Dept. of Electrical Engineering, Division of Biomedical Engineering, Danish Technical University, Ørsteds Plads, Bldg. 349, 2800 Kgs. Lyngby, Denmark (E-mail: chc@elektro.dtu.dk).

0022-3077/09 $8.00 Copyright © 2009 The American Physiological Society

Downloaded from jn.physiology.org on October 22, 2009

outlined in the Guide for the Care and Use of Laboratory Animals, published by the Canadian Council for Animal Protection.

Animal preparation

Details on surgical procedures, electrophysiological methods, and homeostatic measures used in the present study can be found in previous reports from this laboratory (Capaday and Rasmusson 2003; Capaday et al. 1998; Ethier et al. 2006a; Schneider et al. 2001, 2002). Briefly, the animals were anesthetized with an intramuscular injection of ketamine (33 mg/kg) and xylazine (1 mg/kg). Once the surgical procedures terminated, a perfusion pump was connected to a cannula in the femoral vein, and a steady flow of anesthetic (10–30 mg/h ketamine, depending on the animal) was delivered throughout the experiment. The blood pressure recorded from the femoral artery was maintained at ~100 mmHg. The animal's temperature was kept near 37°C by a heating blanket wrapped around the animal's trunk and by an overhead heat lamp. A long skin incision was made to expose the muscles of the left forelimb and shoulder. A pair of multi-stranded, stainless steel wires, separated by ~1.5 cm, was inserted in 8–10 of the following muscles, depending on the animal: the flexor digitorium profondus (FDP), the flexor carpi radialis (FCR) and palmaris longus (PL), extensor carpi radialis longus and brevis (ECRl, ECRb), the lateral head of the triceps (TriL), the brachialis (Br), the clavobrachialis (CBr), the biceps (Bi), the teres major (TM), the latissimus dorsi (LD), the spinodeltoid (SpD), the pectoralis major (PMj), and the pectoralis minor (PMn). The EMG signals were amplified by a factor of 1,000, high-pass filtered at 20 Hz, rectified, and low-pass filtered at 1,000 Hz.

Outline of experimental procedures

Following preparation of the animal, the output of a randomly selected motor cortical point was determined by microstimulation and EMG recordings. Once its output determined, biocytin (Molecular Probes) was iontophoretically ejected from a micropipette having a tip diameter of ~4 μm. The tracer was ejected at a depth of 800 and 1,500 μm from the surface for 30 min. This allowed us to stain neurons in upper layers II–III and the deep layers V–VI or what may be roughly termed a cortical column. The tracer was ejected using a positive current of 300 nA pulsed every 2 s with a 50% duty cycle and superimposed on +50 nA of DC current. Microstimulation mapping was done in two of the animals >8 h after iontophoretic injection of biocytin so as not to potentially interfere with its transport.

Microstimulation procedures

Stainless steel microelectrodes ranging in impedance from 500 kΩ to 1 MΩ were used to microstimulate the motor cortex (area 4γ). Trains of stimuli 50 ms in duration were delivered at random intervals of between 2.5 and 7 s in layer V of the right motor cortex. The duration of single pulses was 0.2 ms, and the rate was usually set at 333 Hz. The microstimulation evoked EMG activity of each point was determined for stimuli near motor threshold (MT) and at 1.5 $\times$ MT. Currents as low as 10 μA evoked visible twitches, and threshold values were typically between 10 and 20 μA. Stimulus currents never exceeded 60 μA. To minimize potential damage of axon collaterals by excessive penetrations, the distance between microstimulation points was set at 1 mm.

Histological processing

Animals were left to survive for 18 h after injection of biocytin at which time under deep pentobarbital anesthesia, the animal was perfused intracardially with 1 l saline containing 1,000 UI of heparine and 0.1% (wt/vol) sodium nitrate. This was immediately followed by perfusion of 2 l of tissue fixative containing 0.1 M phosphate buffer, 4% formaldehyde, 0.3% glutaraldehyde at a pH of 7.4. A block of tissue containing the motor cortex was removed immediately after fixation, flattened between two metal blocks, and placed in a container filled with the fixative. Horizontal sections 80 μm thick were cut from the tissue block several days later in an oscillating microtome. Biocytin was revealed using the Vectastain ABC kit pk-6100 (Vector Laboratories) following standard techniques, with DAB-Ni as the chromogen in the final step (e.g., Capaday et al. 1998; Izzo 1991). A series of sections was mounted on glass slides for optical microscopy, and a separate series was prepared for electron microscopy as described in the following text. The Prussian blue method was used to estimate the tissue shrinkage resulting from perfusion. Briefly, Fe^{2+} ions were deposited from the tip of a stainless steel electrode at a depth of 600 μm at each of four cortical points a known distance apart. The tissue shrinkage was thus determined to be ~25%.

Light microscopy and reconstruction procedures

The outline of one of six tissue sections was drawn at low magnification ($\times$25) taking particular care to identify landmarks such as blood vessels, the contours of the section and the position of the cruciate and coronal sulcii. Axon collaterals emanating from the injection site were then traced at higher magnification ($\times$250) on this outline using the described landmarks for alignment. Six sections per hemisphere were used to reconstruct the axon collateral projections. Additionally, three of these six sections having the highest density of light microscopy identified boutons were selected. The sections were taken from the upper layers II–III and the deep layer V. The position of synaptic boutons was marked on the same section outline as used for tracing the axon collaterals. The criteria used to identify the synaptic boutons under light microscopy at $\times$400 magnification were as follows. The bouton was clearly visible along with the axon segment to which it belongs, and it had to be clear that the element in question was not a dendritic spine or tissue debris. To determine the density of synaptic boutons a grid was drawn on tracing paper, each grid element represented an area of 83 $\times$ 83 μm. The tracing paper was superimposed on the final drawing, and the number of boutons contained in each grid element counted. At each grid element a filled black circle the diameter of which was proportional to the bouton density was drawn on the tracing paper. The axon collateral and synaptic bouton density tracings were digitized on a large commercial scanner.

Electron microscopy

The animals were perfused with a fixative as described in the preceding text. Sections, 50 μm thick, were cut on a Vibratome (Leica V1000), washed with PB and Tris-buffered saline (TBS; 0.05 M Tris buffer, pH 7.4, containing 0.9% saline). After extensive washes, the sections were cryoprotected in 30% sucrose in 0.1 M PB and freeze-thawed in aluminum-foil boat over liquid nitrogen to enhance the penetration of reagents without destroying the ultrastructure. Sections prepared for light microscopic examination were treated with 0.5% Triton X-100 diluted in 0.05 M TBS. Following extensive washes with buffer, sections were incubated in avidin-biotinylated horseradish peroxidase complex (Elite ABC, Vector, 1.5 h, 1:200). The immunoperoxidase reaction was developed using 3,3′-diaminobenzidine (DAB; Sigma) intensified with ammoniumnickel-sulfate (DAB-Ni) as a chromogen. The reaction was triggered by adding 0.003% H_2O_2 to the DAB-Ni solution. For electron microscopy examination, sections were treated with 1% OsO_4 for 1 h, dehydrated in ethanol and propylene oxide, counterstained with uranil-acetate, and embedded in Durcupan. Areas innervated by biocytin-labeled axons were selected and reembedded for ultrathin sectioning. Serial ultrathin sections were cut and mounted on single-slot Formvar-coated copper grids (Sigma, St. Louis, MO). The ultrathin sections were counterstained by lead citrate and examined by a Tecnai 12 electron microscope.

Downloaded from jn.physiology.org on October 22, 2009

Quantitative analysis

The two-dimensional (2D) spatial distribution of boutons was quantitatively analyzed to detect the presence of spatial groupings or clusters. To this end, the count at each grid element of the bouton distribution map of each animal was entered into a data matrix. Three separate but mutually reinforcing multivariate data analysis methods were used. Each data matrix was analyzed by K-means cluster analysis, covariance analysis, and eigenvalue decomposition. Clustering, using the K-means algorithm is a partitioning method that groups together objects that have similar properties, such as for example color (Bishop 2006). In the present context, K-means will group together spatial locations that have similar boutons densities. K-means treats entries in the data matrix as objects having locations and distances from each other. It partitions these objects into *K* mutually exclusive clusters such that, objects within a cluster are as close to each other as possible and as far as possible from objects in other clusters. Each cluster is characterized by its barycenter, the weighted average of the coordinates of the data points. For a finite data set, the algorithm is guaranteed to converge to a solution. The presence of large clusters does not preclude identification of smaller clusters because clusters are defined as objects having similar properties. Thus the presence of a large cluster having the property of say red does not affect the algorithm in finding smaller clusters of say green. Unlike some other clustering algorithms, such as the mean-shift algorithm (Binzegger et al. 2004), the dataset does not need preprocessing, and no a priori decision is required on the number of clusters thought to be in the data. The mean-shift algorithm does not provide information on whether the identified clusters are significant from a statistical point of view. With K-means, one can get a quantitative measure of the quality of the clustering using silhouette plots as will be described in RESULTS. Another way to identify the presence of bouton clusters is to determine the number of modes, or peaks, in the bouton distribution map. The covariance matrix gives the covariance between all combinations of rows, or columns, of the data matrix. It represents the lag-zero covariance between spatial locations. The covariance matrix can be represented as a 3D surface, with the *x*-*y* plane representing spatial location and the *z*-axis the covariance at that location. Strong spatial clustering of boutons would result in a multi-peaked 3D surface. Conversely a monotonically decreasing bouton density would result in a unimodal surface. Additionally, the covariance of the bouton distribution at different spatial lags can reveal the presence of peaks in the map that may not be evident in the zero-lag covariance matrix. Thus if a cluster of boutons exists at a certain location, then a peak in the cross-covariance functions will appear at the spatial lags covering that location. Finally, we also determined the eigenvalue distribution of the data covariance matrix. By sorting the eigenvalues in decreasing order, known as a scree plot, one can determine significant rupture points in the eigenvalue distribution. The presence of significant clusters in the data would be revealed by the number of significant eigenvalues. Thus for example, a unimodal distribution will have one significant eigenvalue and the 3D representation of the covariance matrix will be unimodal. Conversely, a multimodal distribution of boutons (i.e., clustered) would result in a number of significant eigenvalues equal to the number of peaks in the distribution.

RESULTS

MCx neurons give rise to an extensive network of horizontal axon collaterals

The anterograde tracer biocytin was ejected iontophoretically in layers II, III, and V of the motor cortex. This stained some 30–50 neurons within a radius of ~250 μm (Fig. 1, *A* and *B*). Note the labeled somas at the injection site and the fine axon collaterals that emanate from the somas. Only two poorly labeled somas were found away (>300 μm) from the injection center in the three animals examined. This demonstrates that the vast majority of the observed axon collaterals were labeled anterogradely. A series of terminations—or boutons en passant—are observed along the axonal branches (Fig. 1*C*). These terminations appear as varicose swellings of the axon or as swellings at the tip of fine stalks (Fig. 1*C*). Figure 2 shows the extensive network of horizontal axon collaterals that emanate from the injection site. The collaterals extend into nearly all of the forelimb representation area of the motor cortex and caudally into the primary sensory cortex. The microstimulation mapped right motor cortex (Fig. 2*A*) shows a distribution and density of labeled fibers similar to that of the left motor cortex, which was not mapped (*B*). Thus the numerous penetrations required to map the motor cortex did not significantly affect the quality of the labeling. No axonal clusters similar to those found in layer III of the primary visual cortex were observed (e.g., Bosking et al. 1997; Buzas et al. 2006).

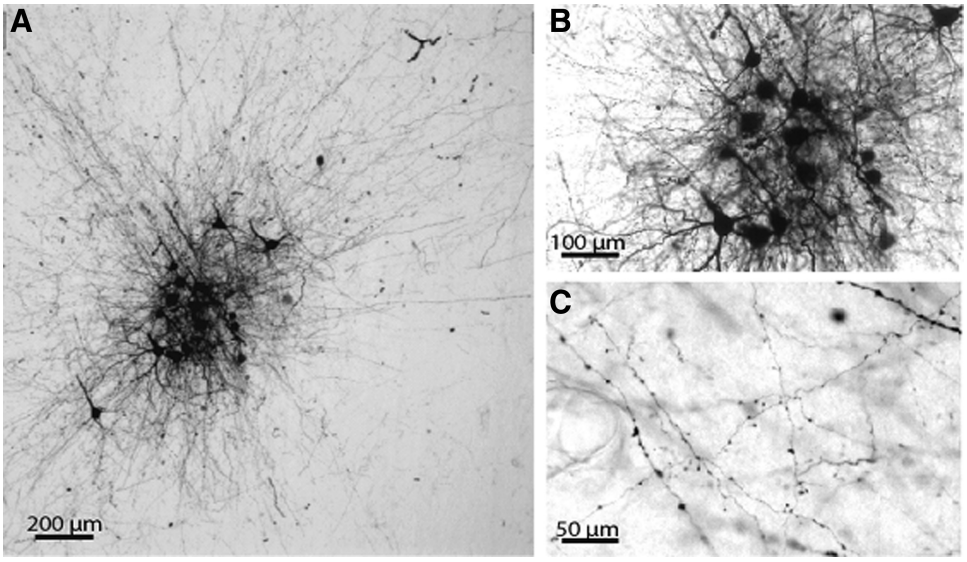

FIG. 1. Photomicrographs of biocytin-labeled neurons at different magnifications. *A*: in this horizontal section, note the labeled somas at the injection site and the fine axon collaterals emanating from the somas. *B*: the somas of the same group of neurons at higher magnification. *C*: note the club-like swellings (boutons) all along the fine axon collaterals. Data obtained from *animal C99-10.*

Downloaded from jn.physiology.org on October 22, 2009

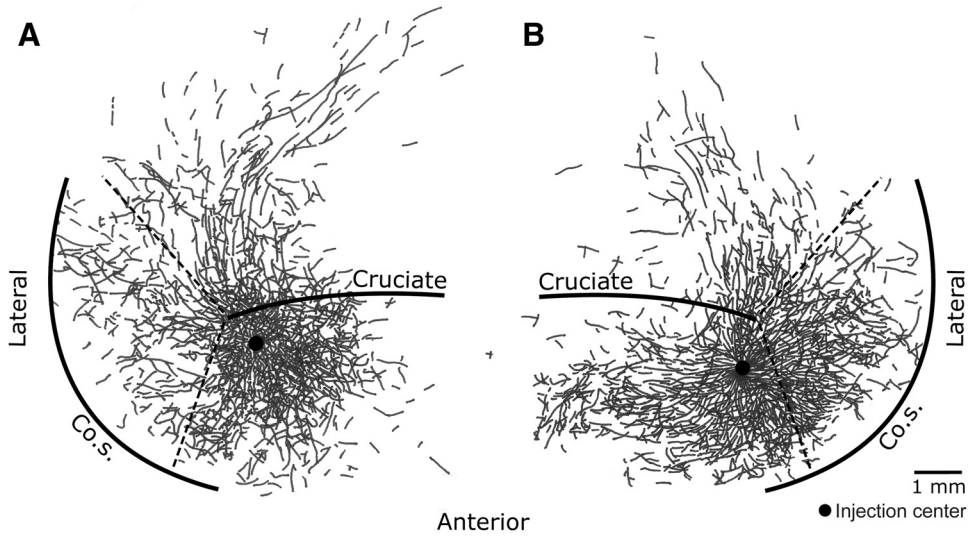

FIG. 2. Pyramidal cells of the cat motor cortex give rise to an extensive network of horizontal axon collaterals. The motor cortex is bounded laterally by the coronal sulcus (Co.S.). - - -, the location of the coronal gyrus (see Fig. 3). The areas anterior and posterior to the cruciate sulcus, respectively the anterior and posterior sigmoid gyri, along with the coronal gyrus constitute the cat primary motor cortex. Area 3a is typically situated some 5–10 mm posterior to the cruciate sulcus. Biocytin was injected in points marked by a dark circle. Threshold level microstimulation at that point evoked activity in the Br in A and the ECR in B. *A*: the microstimulation mapped right motor cortex shows a distribution and density of labeled axon collaterals comparable to that of the unmapped left motor cortex shown in *B*. Data obtained from *animal C06-4*.

Horizontal axon collaterals are studded all along their course with boutons

The bouton density map reconstructed across the expanse of the motor cortex of two animals is shown in Fig. 3. The bouton density map of the third animal was qualitatively similar. In Fig. 3*A*, biocytin was injected in a motor cortical point at which microstimulation at threshold intensity evoked a motor response in the LD and in *B* in the Br. The bouton density is highest around the injection center forming an elongated region of $\sim 1 \times 2$ mm. It is important to note that the distribution of boutons in Fig. 3*A* has a pattern similar to that of the axon collaterals in Fig. 2*A* from which it is derived. The boutons, like their parent axon collaterals, cover nearly all of the forelimb representation in the motor cortex. There are no obvious areas of high-density bouton counts beyond the central high-density core. The bouton density decreases gradually from the injection center (Fig. 4). In these three-dimensional (3D) surface plots, the small conical peaks at long distances from the center should not be interpreted as evidence of bouton clustering. They are the result of a limited sampling of the tail of the distribution. This is because the axon density per unit volume decreases with distance from the injection center, akin to the way electric field line density decreases for a point charge. Near the center of the injection because the density is relatively high, counting over a limited number of sections fills in the area, but in the periphery, because the density is inevitably lower, counting over the same number of sections will not fill out the area. There will be large areas with little or no counts and a smaller number of areas where counts exceed zero. The 3D rendering thus gives the appearance of small isolated conical peaks. A clustered distribution as observed for layer II–III neurons in visual cortex (e.g., Bosking et al. 1997; Buzas et al. 2006) would result in peaks of roughly comparable size over large distances which rise well above the background. By contrast, the conical peaks in Fig. 4 decrease progressively with distance. Importantly, the counts represented by the distant conical peaks in Fig. 4 are of the order of between one and four boutons per bin, whereas the boutons clusters in visual cortex contain several hundred to thousands of boutons covering areas of some $5–6 \times 10^4$ μm^2. Moreover, the boutons clusters in visual cortex recur with a periodicity of between 500 and 1,200 μm (Bosking et al. 1997; Buzas et al. 2006). There is no periodicity in our bouton distribution map. The mathematical analyses presented in the next section provide quantitative evidence that the bouton distribution is unimodal, meaning that bouton density decreases progressively with distance from the injection site. By contrast, as noted in the preceding text, clustered distributions such as found in visual cortex are multipeaked (Binzegger et al. 2004).

Multivariate analyses demonstrate a unimodal distribution of synaptic boutons

A K-means cluster analysis of the data matrix representing the spatial distribution of boutons was done using the Matlab KMEANS function and squared Euclidean distances. The desired number of clusters was initially set to two. A typical result is shown in Fig. 5, *A* and *B*, as cross views along the horizontal and vertical axis respectively. The coordinates of the axes represent bin location along that axis. It is apparent that the bouton map is clearly partitioned into two zones, a high-density zone corresponding to a circle centered at coordinates (60, 65), surrounded by a low-density zone. The class having index 1 corresponds to the low-density zone, whereas the class having index 2 represents the high-density zone. The results of a 3-class K-means clustering analysis are presented in Fig. 5, *D* and *E*. The region having class index 3 corresponds to the high-density region. Moreover, the class index 2 region has a ring shape around the main peak (Fig. 5, *D* and *E*), corresponding to an intermediate bouton density and to the significant part of the tail of the bouton distribution. The class 1 region in the three-class partition corresponds to locations having no or very few boutons counts. To determine how well separated the clusters are, silhouette plots were constructed (Fig. 5, *C* and *F*). A silhouette value ranges between ± 1 and is a measure of how similar a cluster member is to members of the same cluster compared with members of other clusters. A negative value is indicative of poor clustering because it implies that a particular member is closer to members of other clusters than to those of its cluster. In the silhouette plot of Fig. 5*C*, it can be seen that most points in the bigger cluster (index 1) have values >0.8, indicating that they are well separated from neighboring clusters. For this cluster, the silhouette plot shows a few points with

Downloaded from jn.physiology.org on October 22, 2009

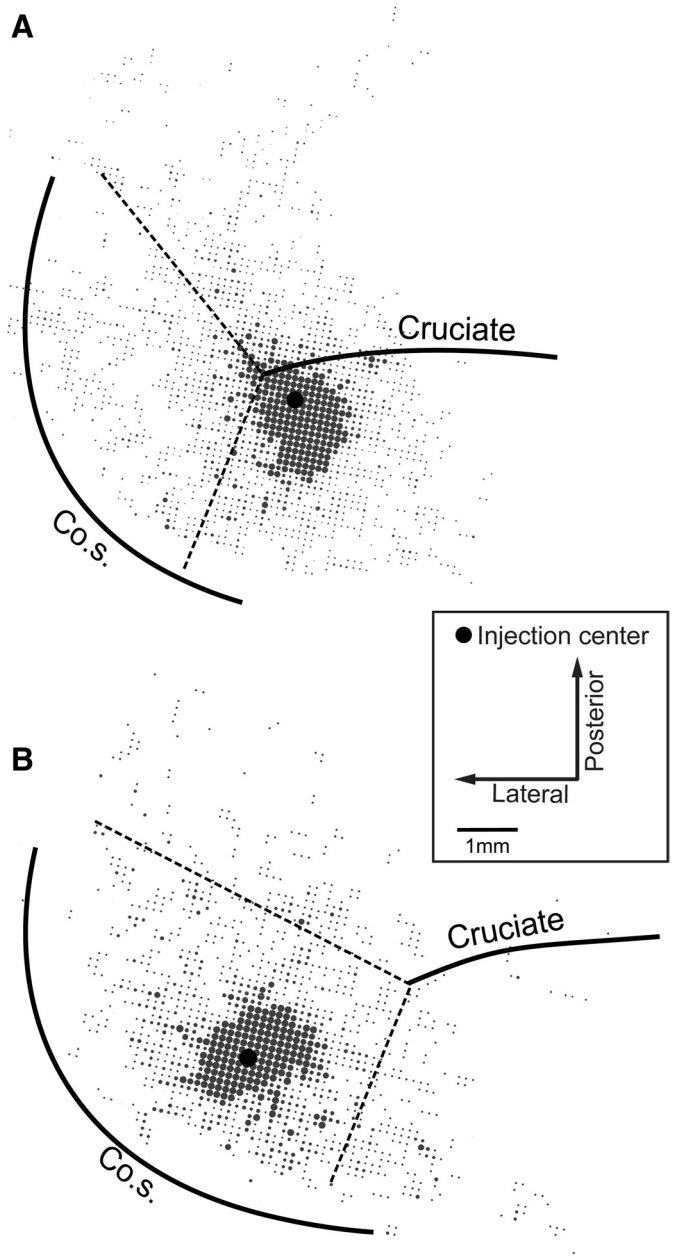

FIG. 3. Distribution of boutons along the axon collaterals of neurons labeled at the injection site (dark circle). The size of each dot is proportional to the number of boutons in a grid element of 83 × 83 μm. *A*: from *animal C04-4,* the same animal the axon collateral distribution of which is shown in Fig. 2, *A* and *B,* from *animal C06-4.*

low or negative values (Fig. 5*C*), indicating that they are close to points in other clusters. These points correspond to locations in a "transition ring" having an intermediate number of boutons. The result of partitioning the bouton map into three clusters is shown in Fig. 5*F*. The number of negative values increased considerably and the separation between clusters decreased. It can be seen that the new cluster (index 3) has a poor average silhouette value of ~0.37. Because the data matrix is relatively sparse, most of the matrix entries have a low or zero value. Therefore if there were only two clusters in the bouton map, a partitioning involving more than two clusters will result in a large number of points having low or negative silhouette values. These considerations suggest that the best partitioning of the bouton maps is in only two clusters. What is important is that the K-means partitionings (Fig. 5, *A–D*) have a concentric rings shape typical of the topology of monotonically decreasing unimodal distributions. This conclusion is reinforced by the lagged covariance function analysis and eigenvalue decomposition presented next.

Another way to search for the presence of clusters is to determine the number of modes, or peaks, in the bouton distribution map. To this end, the covariance matrix was calculated between the rows of the data matrix and the columns of its transpose, for all three bouton maps. Figure 6A shows an example of a covariance matrix represented as a 3D surface plot as explained in METHODS. The single-peaked nature of the plot is striking. Note also that the smoothing effect of the covariance function attenuates the data variability, or what is equivalently uncorrelated data (compare Fig. 6*A* with Fig. 4*B*). An example of the lagged covariance functions is shown in Fig. 6*B*. Each lag value represents displacement by one bin of the bouton map or one element of the data matrix. Apart from the main peak the width of which is commensurate with the central high-density region, typical side lobes can be seen due to the finite size of the data matrix (i.e., similar to convolution of a signal with a rectangular window). Clearly, the plots shown in Fig. 6 indicate that the spatial distribution of boutons is unimodal, confirming the results of the K-means cluster analysis. Yet another mathematical analysis of the data matrix involved determining the eigenvalues of its covariance matrix and sorting them in decreasing order. For each of the three bouton distribution maps, only one eigenvalue was found to be significant, accounting for ≥90% of the variance. This is strong additional evidence that the bouton distribution is indeed unimodal.

Electron microscopy reveals that the majority of boutons identified by light microscopy form synapses

Electron microscopy was used to establish the targets innervated by the stained and reconstructed axon terminals. Briefly, sections were examined at high magnification in the light microscope and the location of putative boutons identified and photographed. Chosen areas were re-embedded for subsequent ultra-thin sectioning. The identified putative boutons were analyzed using correlative light and electron microscopy approach (Sik et al. 1995). Ten of 12 light microscopically identified boutons were thus shown to form synapses. In addition randomly chosen boutons were analyzed to determine the nature of postsynaptic targets and the type of presynaptic terminals. The vast majority of boutons (n = 30, 71.6%) formed asymmetric (type I, excitatory) synapses on dendritic spines (Fig. 7*A*) with single release sites. On rare occasions (n = 2, 4.7%), a single bouton innervated two individual spine heads (Fig. 7*B*). Asymmetrical synapses (n = 4, 9.5%) also were found on dendritic shafts of presumably inhibitory cells. Symmetrical synapses (type II, presumed inhibitory terminals) were also found (n = 6, 14.2%) innervating dendritic shafts (Fig. 7*C*). The results of the electron microscopic analysis are summarized in Table 1.

Downloaded from jn.physiology.org on October 22, 2009

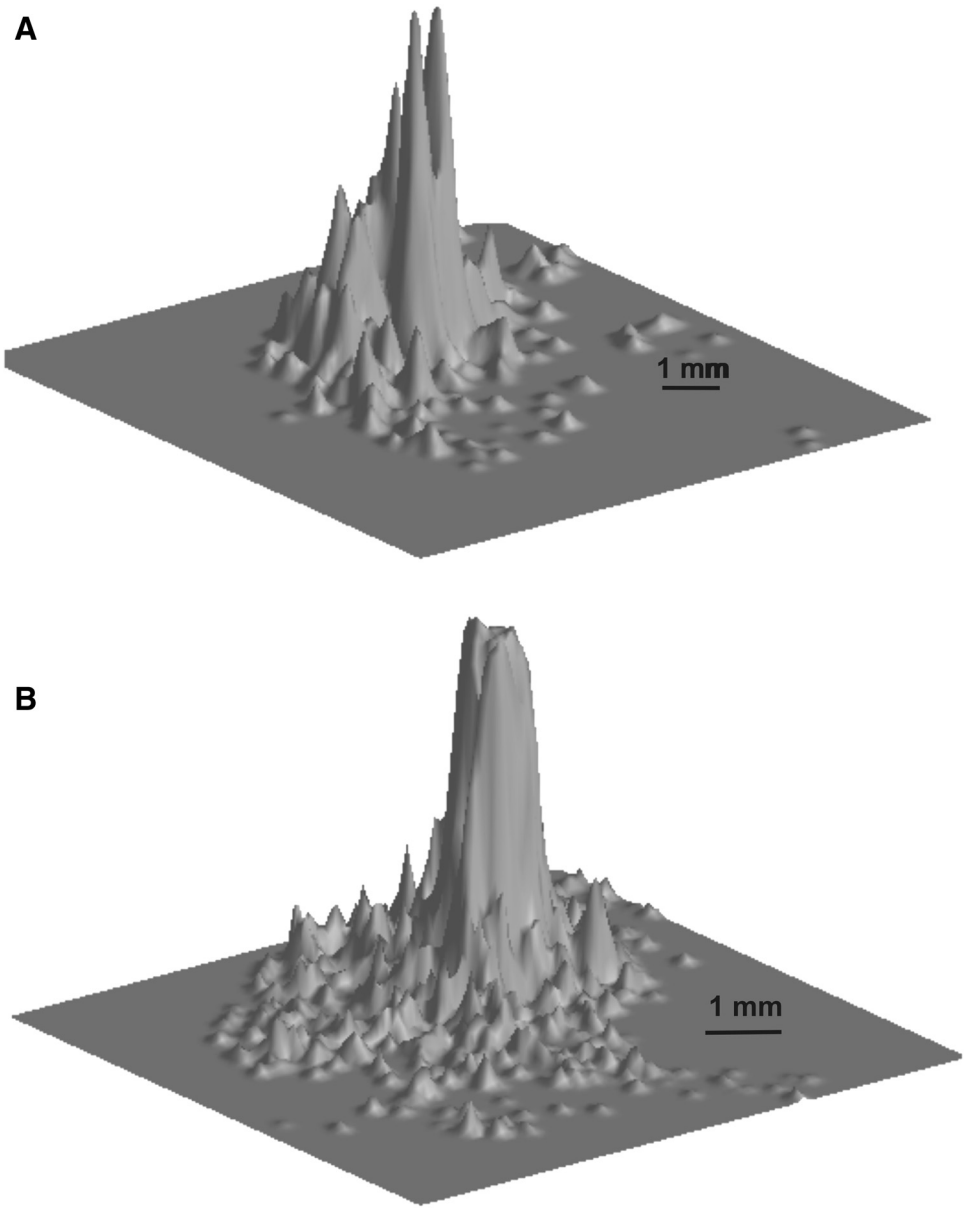

FIG. 4. The bouton density maps shown in Fig. 3 are displayed here as a 3-dimensional (3-D) surface plots using the Matlab surfl function. The data matrix containing the bouton counts was smoothed with a 5 × 5 Gaussian kernel (SD = 0.625 pixels), before plotting. The peak bouton density is 54 boutons in *A* and 60 boutons in *B*, each in a grid element of 83 × 83 μm. Note that bouton density decreases approximately monotonically with distance from the injection site.

Distribution of boutons across the MCx binds together a variety of muscle representations

The reconstructed bouton density maps were superimposed in register with the microstimulation derived muscle maps. An example is shown in Fig. 8, where the microstimulation derived muscle maps obtained at 1.0 and 1.5 × MT are superimposed on the bouton density map of that animal (Fig. 3*A*). Three features of the muscle representation maps and their relation to the bouton distribution map are noteworthy. First, it is clear that a given muscle is represented at widely separate and noncontiguous points and that it is true for both proximal (e.g., LD) and distal muscles (e.g., EDC). A feature of motor cortical organization that has been extensively reported (e.g., Sanes and Schieber 2001; Schieber 1999; Schneider et al. 2001). Second, a large number of cortical points represent more than one muscle, even for responses evoked at threshold. The greater number of cortical points representing more than one muscle at 1.5 × MT versus 1.0 × MT is not simply the result of current spread because novel responses appearing at 1.5 × MT are not always predictable from responses of surrounding points obtained at 1.0 × MT. For example, in the muscle map obtained at 1.0 × MT the ClBr muscle is represented only once medially in the anterior-most row (Fig. 8*A*). However, at 1.5 × MT, it appears at widely different and noncontiguous loci in combination with both distal (e.g., EDC) and proximal muscles (e.g., LD). Similarly no responses were evoked in the Br at 1.0 × MT. However, at 1.5 × MT responses were evoked in the Br from widely spaced and noncontiguous loci in combination with both proximal and distal muscles. Third and most importantly, the bouton density map covers a heterogeneous muscle representation map (Fig. 8). The muscles represented span the forelimb from digit to shoulder. It is clear from Fig. 8 that the boutons are not restricted to areas in which the LD is represented (i.e., the muscle represented at the point where biocytin was injected). They are also found in areas where the shoulder muscle ClBr

Downloaded from jn.physiology.org on October 22, 2009

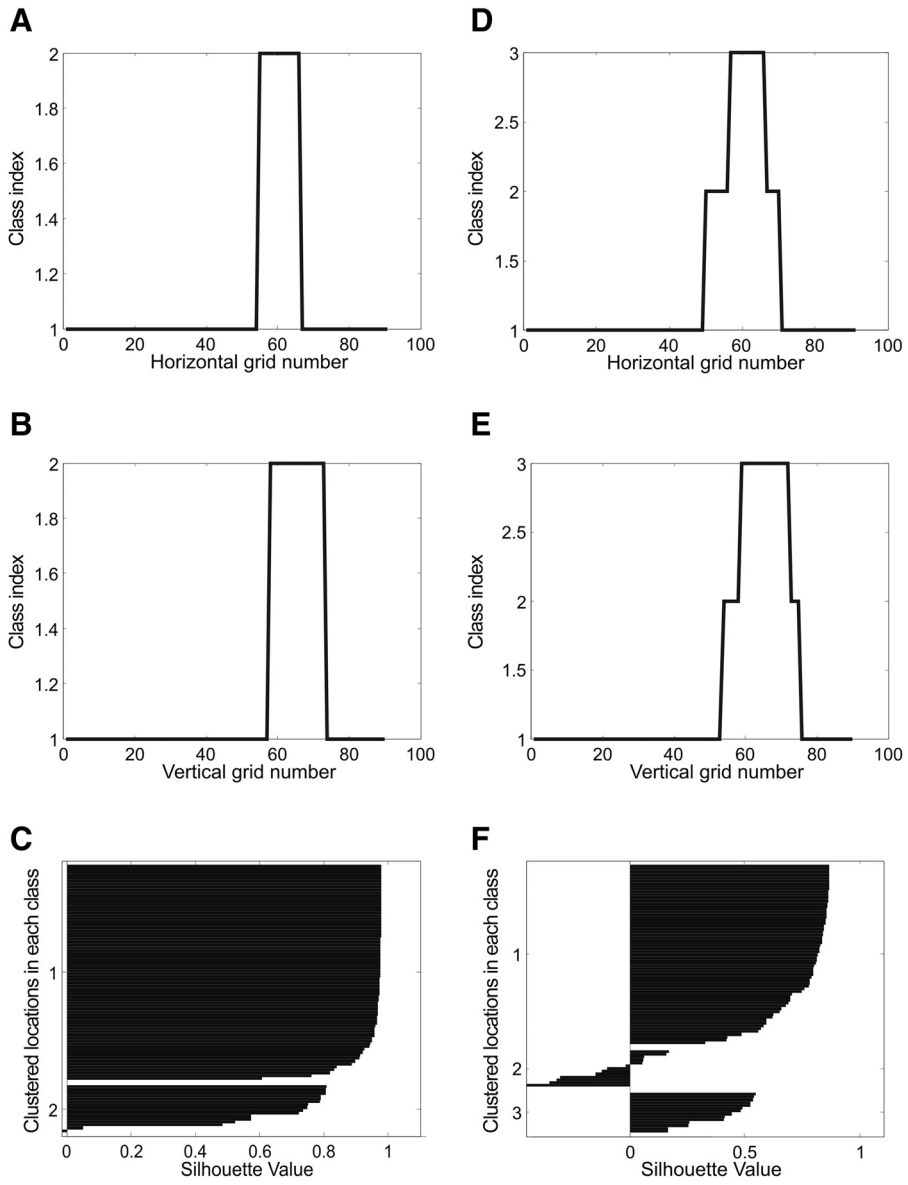

FIG. 5. Example of the clustering analysis of data obtained from *animal C04×4*. Class index values of the K-means 2-class clustering analysis are presented in *A* and *B* and in *D* and *E* for the 3-class clustering analysis. The axes represent the orthogonal directions of rows and columns along the data matrix. Silhouette plots for a 2- and 3-class clustering analysis are shown is *C* and *F*, respectively. Details on the interpretation of these graphs are provided in the text.

is represented, the elbow muscle Br, the wrist muscles ECR and PL/FCR and the digit muscle EDC. The observation is equally valid when considering the area of highest bouton density, or the map as whole.

DISCUSSION

The intrinsic connections of a cortical area outnumber its feedforward and top-down (feedback) connections (e.g., Dayan and Abbott 2001; White 1989). Understanding the function of intrinsic connections is therefore fundamental to understanding the neural processing occurring within a cortical area. Predicated on this idea we linked anatomy and physiology in finer detail than previous studies on the subject (Huntley and Jones 1991; Keller 1993). Motor output was measured by intramuscular EMG recordings from up to 10 muscles making for a detailed motor map. Axonal collaterals were traced from origin to termination with special care to identify the synaptic boutons along their course using correlative light and electron microscopy. Superposition of the synaptic bouton distribution map and the motor output map revealed that motor cortical neurons don't make point-to-point connections but rather bind together the representations of a variety of muscles within a large neighborhood. Thus any cortical point may potentially influence any other cortical point within its innervation territory. This would allow for synergistic interactions between arbitrary cortical points giving rise to a rich repertoire of possible movements. These issues are discussed further in the following text.

The intrinsic connectivity pattern of the cat MCx we describe is consistent with White's canonical cortical circuit principles (White 1989). His first principle states "every neuron in the target region of a projection receives input from the projection" and, importantly, its corollary states that "axon terminals from any extrinsic or intrinsic source synapse onto every morphological or physiological neuronal type within their terminal projection field. . . ." We have shown that excitatory and inhibitory neurons in a large region surrounding the injection site receive inputs from that site. Our data do not

Downloaded from jn.physiology.org on October 22, 2009

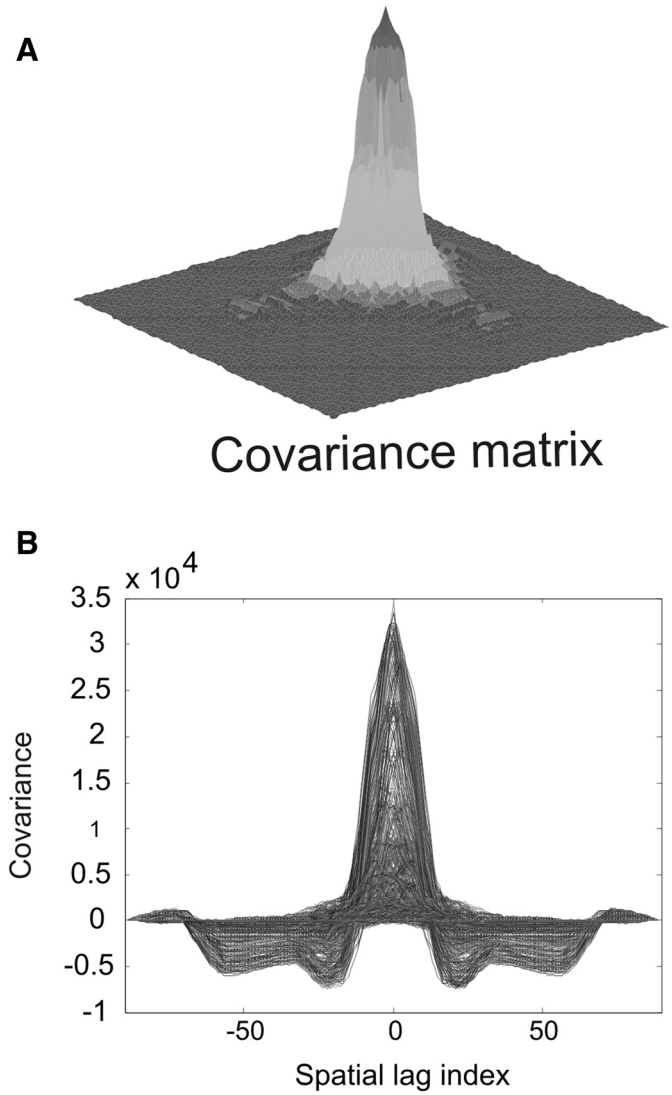

FIG. 6. The covariance matrix (0 lag) of the bouton distribution matrix is plotted as a 3-D surface plot in *A*. The *z* axis represents the covariance value between all rows and columns of the bouton distribution matrix. Note the striking single-peaked (unimodal) nature of the covariance matrix. Superimposed plots of the lagged-covariance functions are shown in *B*. The autocovariances and cross-covariances are superimposed in this plot. The covariance matrix shown in *A* represents all possible covariances at 0 lag in *B*. Note again the striking single peaked nature of the cross-covariance functions. The data analyzed are the same as that of Fig. 5. Further details are given in the text.

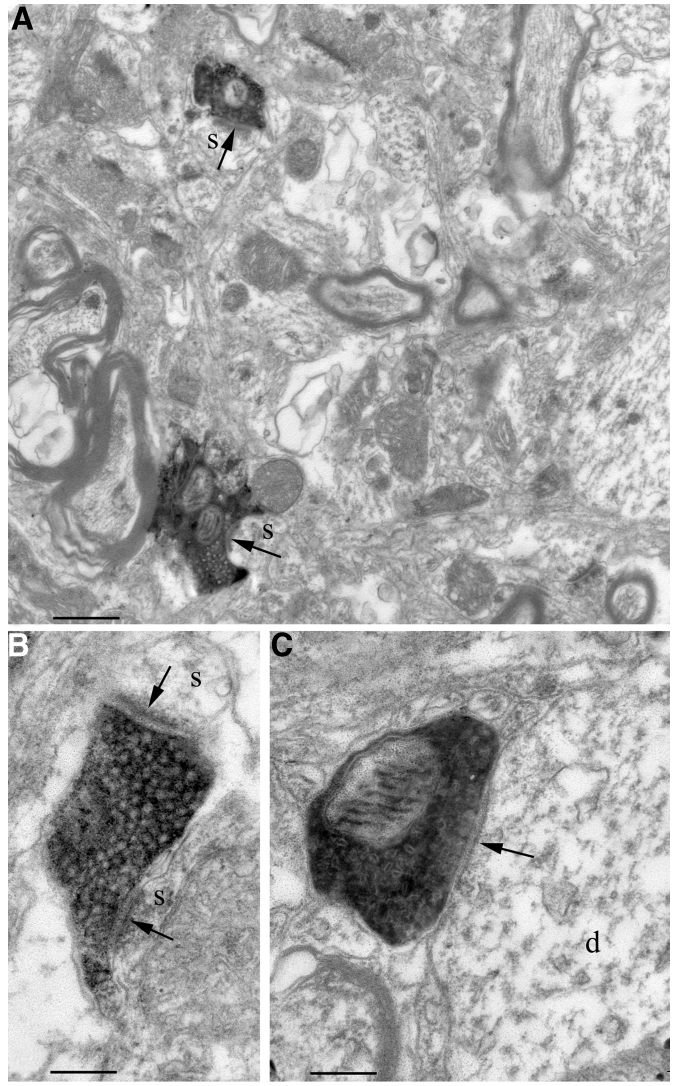

FIG. 7. Targets of biocytin-filled axon terminals. *A*: the vast majority of labeled boutons (black profiles) terminate on spines (s) forming asymmetrical synapses with single release sites (arrowheads). *B*: occasionally a single bouton forms asymmetrical terminals on 2 spines. *C*: in rare occasions, labeled boutons form symmetrical synapses on dendritic shafts (d). Scale bars: *A,* 500 nm; *B* and *C,* 200 nm.

allow us to confirm that every neuron in this extended region covering nearly all of the forelimb representation receives input. But it does show that neurons throughout the projection region do (Figs. 2 and 3). Hopfield networks and other recurrent networks are fully interconnected (Dayan and Abbott 2001) such that the output of any one unit feeds the output of all other units. Notwithstanding the potential caveat regarding White's first principle, the connectivity pattern of the motor cortex resembles that of recurrent networks in which the output connections from a motor cortical point are made onto surrounding excitatory as well as inhibitory neurons. This network topology is consistent with a balanced cortical network suggested by Van Vreeswijk and Sompolinski (1996) for which there is now experimental evidence (Ethier et al. 2006a; Haider et al. 2006). The recurrent network pattern of the intracortical connectivity strongly supports the hypothesis that the MCx controls the musculature in an integrated manner; that is, muscles are not controlled individually but in functional groups (Capaday 2004; d'Avella et al. 2006; Devanne et al. 2002; Gentner and Classen 2006). However, recurrence is probably one of many to be discovered network topology principles.

Our study and those of Huntley and Jones (1991) in the monkey and Keller (1993) in the cat unequivocally demonstrate strong intrinsic connectivity between widespread areas of the MCx. However, there are also differences in detail and interpretation between these studies and ours that are important

TABLE 1. *Summary of the electron microscopic analysis*

No. of Boutons on	Asymmetric, %	Symmetric, %
Spines	72 (32)	0
Dendritic shafts	13 (4)	15% (6)

n values in parentheses.

Downloaded from jn.physiology.org on October 22, 2009

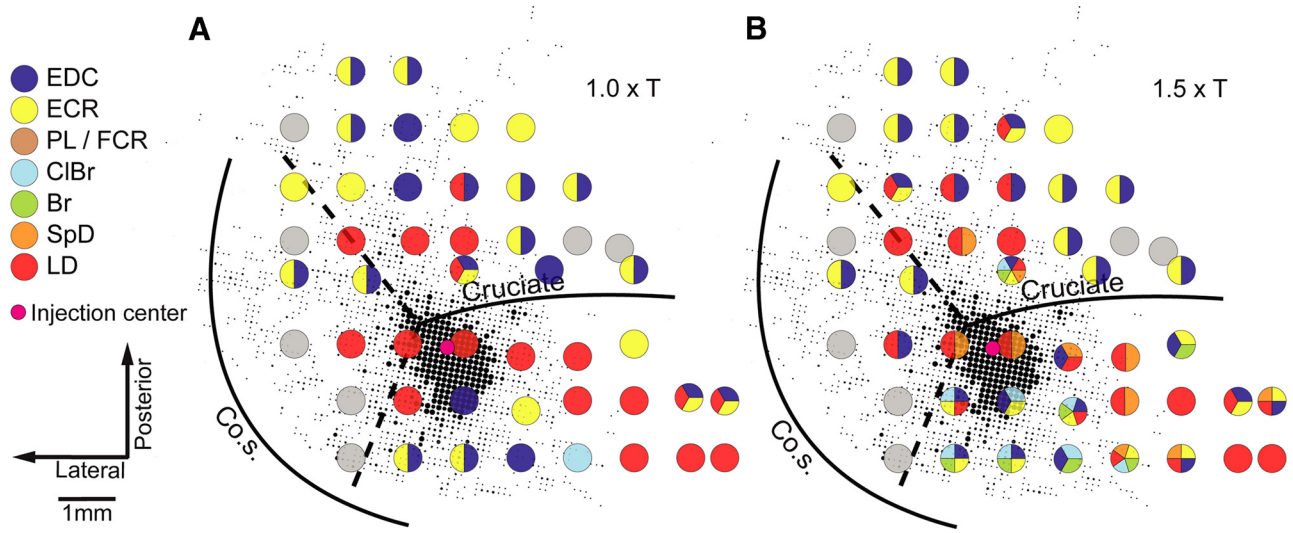

FIG. 8. Superposition of the bouton density map on the microstimulation-derived muscle map. Evoked muscle responses at each point at which microstimulation was applied are represented by the color code of the legend (*left*). Gray circles represent points at which no response was obtained (NR). Note that at many cortical points >1 muscle was recruited. *A*: the microstimulation derived muscle map at 1.0 × T. *B*: the muscle map obtained at 1.5 × T. Data obtained from *animal C06-4*.

for elucidating the nature of the connectivity pattern and its functional role. The emphasis of their reconstructions was on terminal fiber labeling without explicitly defining what these may be and implicitly assuming that boutons are only found there. Both studies emphasize "a distinctly patchy" distribution of these so called terminal fibers. However, the spatial distribution of synaptic boutons shown in Fig. 4 is not consistent with this interpretation. Synaptic boutons do not show a patchy distribution in the motor cortex, rather their density decreases roughly monotonically with distance from the site of injection. Moreover, the bouton distribution closely matches the course of the axon collaterals (compare Figs. 2*A* and 3*A*). The patchiness reported by previous authors may be due to incomplete staining or reconstruction. By contrast, we carefully traced the axonal projections from their origin to their termination across several sections. Care was also taken not to confuse en passant boutons from thickenings containing aggregation of mitochondria, which was confirmed by correlative light and electron microscopy. The monotonic decrease of bouton density we found in the cat MCx is consistent with a recurrent network organization in which connection strength decreases with distance between units. A patchy distribution pattern is more consistent with a point-to-point connectivity. The mathematical analyses we applied to the bouton distribution map do not demonstrate a patchy, or clustered, distribution. More importantly, the emphasis on descriptions of terminal fiber labeling suggests that there are very few connections between neurons in a radius of ~1.5–2 mm around a cortical point (e.g., see Fig. 9 in Huntley and Jones 1991). Whereas it is clear that the connection density is greatest within this area as demonstrated by the bouton density map (Fig. 5).

The characteristics of reconstructed single layer V neurons (Capaday 2004) lend further support to our recurrent network idea. Their axon collaterals are studded with synaptic boutons all along their course. Moreover, in the example shown in Fig. 3 of Capaday (2004), there are no obvious terminal arborizations, or axonal tufts. Note that even for branches that terminate relatively closely to the soma terminal tufts are absent, while the axon was stained ≤6 mm away from the soma. It is therefore extremely unlikely the absence of terminal arborizations and tufts in that example, or in the present material, is due to incomplete staining. The axonal arbor of cat MCx neurons thus resemble those of hippocampal pyramidal neurons (Sik et al. 1993). Clearly the absence of terminal arborizations, or axonal tufts, does not entail absence of connectivity. Perusal of the relatively few studies of axonal branching of MCx neurons (e.g., Capaday 2004; Ghosh et al. 1988; Keller and Asanuma 1993; Landry et al. 1980) shows that single neurons of the MCx do not appear to have the striking axonal tufts found in many visual cortex neurons (e.g., Buzas et al. 2006). It stands to reason that connectivity organized in terms of bouton patches cannot be a prominent feature of the cat MCx. The functional organization of V1 in primates and carnivores differs from that of MCx in several respects. In these species, there is a clear functional modular organization, including a retinotopic map, orientation selectivity maps, and ocular dominance maps. The nature of the functional organization of MCx remains elusive and does not appear to have the functional modular organization of V1. For example, the representations of spatially distant muscles may be close together, or even overlap, and individual muscles are represented many times over in noncontiguous loci in various combinations with other muscles (Devanne et al. 2006; Donoghue et al. 1992; Rathelot and Strick 2006; Schneider et al. 1997). The difference in the pattern of connectivity between V1 and cat MCx may thus reflect differences in their function and functional organization. Indeed, Van Hoosen et al. (2006) demonstrated that in the gray squirrel, an animal possessing orientation-selective neurons but no orientation maps, the horizontal connections are not patchy. Thus different functional organizations may have different patterns of connectivity. In summary, we have found that in the cat motor cortex the bouton density is greatest in a radius of between 1,000 and 1,500 μm centered on the injection site and decreases approximately monotonically with distance.

Downloaded from jn.physiology.org on October 22, 2009

The idea that emerges from consideration of the present findings is that communication between motor cortical neurons, at least in the cat MCx, occurs by an inclusive broadcast style of communication rather than by private lines (i.e., point to point). That is a cortical point controlling a given muscle(s) communicates its activity to a large neighborhood where a variety of muscles spanning several joints are represented. Consequently, the firing rate of neurons at any one cortical point reflects the activity state of the neighborhood. We suggest that this network state dependence provides appropriate scaling of motor output from each cortical point and anticipation of what additional muscles may need to be recruited as the movement evolves or is perturbed. We have previously shown that experimentally produced ictal bursting at a motor cortical point spreads over a substantial part of the cortical territory covered by the recurrent connections reported here (Capaday 2004; Capaday et al. 2006). Based on a propagation velocity of 0.1–0.2 mm/ms (Capaday et al. 2006), an area of some 3 mm^2 (i.e., 1 mm in radius) would be activated in 5–10 ms. The pre-EMG activity of motor cortex neurons lasts tens of milliseconds (e.g., Cheney and Fetz 1980; Lamarre et al. 1978), thus allowing for extended spatial interactions prior to movement initiation. This spread of activity along the routes of connectivity underscores the importance of inhibition and disinhibition of motor cortical points in the dynamic operation of the motor cortex (Schneider et al. 2002). Without selective inhibitory control, activity at a cortical point would recruit muscles that are not wanted as part of the movement-related muscle synergy. The present results taken together with our study of the effects of disinhibition (Schneider et al. 2002) emphasize the necessity of interplay between excitation and inhibition in the dynamic operations of the motor cortex. Put simply, the massive recurrent connectivity of the motor cortex requires mechanisms for selective recruitment and concomitant stabilization.

The cortical connectivity pattern such as shown in the example of Fig. 8 represents a number of possible functional linkings between the represented muscles. However, different patterns would be observed by injecting an anterograde tracer at other points in this neighborhood. From this perspective a combinatory complex number of possible functional linkings between muscles may exist. Recent studies aimed at elucidating the classic degrees-of-freedom problem of motor control have interpreted the connectivity pattern of the motor cortex as possibly providing a solution by functionally coupling muscle groups into synergies (d'Avella et al. 2006; Gentner and Classen 2006). Physiological evidence of such functional coupling between the cortical representations of task related muscles was previously presented by Devanne et al. (2002). The connectivity pattern of the motor cortex may at some level be related to dimensionality reduction. However, given the nature of this connectivity pattern, there may be more than one solution to the dimensionality reduction problem embedded in the motor cortex. This would be consistent with the large repertoire of possible movements, especially evident in humans. There is a twin challenge here, determining whether the connectivity pattern is related to dimensionality reduction and if so, elucidating the mechanisms by which a particular solution is selected. It is also important to consider that the intrinsic motor cortical connectivity may have its actions reinforced by the extensive intraspinal branching of individual corticospinal axons (McKiernan et al. 1998; Shinoda et al. 1976; Tantisira et al. 1996). For example, experiments using spike-triggered averaging of EMG activity revealed that 50% of corticospinal neurons project to both proximal (e.g., shoulder, elbow) and distal a motoneuron pools (e.g., wrist and hand); some control muscles at three different forelimb segments (McKiernan et al. 1998). Presumably the cortical network allows for more flexible selections of muscle synergies.

Concluding remarks

Is all the "knowledge" of the motor cortex contained in its connections? In the affirmative, this implies that all movement engrams are embedded in its circuitry (e.g., Aflalo and Graziano 2006; Monfils et al. 2005). Alternatively, can flexible selections of motor outputs occur on a moment-to-moment basis as a result of the motor cortex's activation state (Capaday 2004; Schneider et al. 2002)? Such questions will require considerable future investigations. The data reported here lay parts of the foundation by suggesting that that the motor cortex controls the musculature in an integrated manner rather than singly and separately and that there appears to be a substrate for the dynamic selection of motor output patterns.

ACKNOWLEDGMENTS

The expert and dedicated technical assistance of G. Charette, F. Roy, P. Vachon, and P. Lemieux is gratefully acknowledged. We also thank Drs. Martin Deschênes and Zoltan Kisvarday and D. Giguère for comments and suggestions on a draft of the manuscript.

GRANTS

This work was funded by the Canadian Institutes for Health Research to C. Capaday and A. Sik and the Human Frontier Science Program to A. Sik.

REFERENCES

Aflalo TN, Graziano MS. Possible origins of the complex topographic organization of motor cortex: reduction of a multidimensional space onto a two-dimensional array. *J Neurosci* 26: 6288–6297, 2006.

Binzegger T, Douglas RJ, Martin KA. A quantitative map of the circuit of cat primary visual cortex. *J Neurosci* 24: 8441–8453, 2004.

Bishop CM. *Pattern Recognition and Machine Learning.* New York: Springer, 2006.

Bosking WH, Zhang Y, Schofield B, Fitzpatrick D. Orientation selectivity and the arrangement of horizontal connections in tree shrew striate cortex. *J Neurosci* 17: 2112–2127, 1997.

Buzas P, Kovacs K, Ferecsko AS, Budd JM, Eysel UT, Kisvarday ZF. Model-based analysis of excitatory lateral connections in the visual cortex. *J Comp Neurol* 499: 861–881, 2006.

Capaday C. The integrated nature of motor cortical function. *Neuroscientist* 10: 207–220, 2004.

Capaday C, Devanne H, Bertrand L, Lavoie BA. Intracortical connections between motor cortical zones controlling antagonistic muscles in the cat: a combined anatomical and physiological study. *Exp Brain Res* 120: 223–232, 1998.

Capaday C, Ethier C, Brizzi L, Weber DJ. Microelectrode array recordings of spatial activity spread in cat motor cortex. *Soc Neurosci Abstr* 657.4, 2006.

Capaday C, Rasmusson DD. Expansion of receptive fields in motor cortex by local blockade of GABA(A) receptors. *Exp Brain Res* 153: 118–122, 2003.

Cheney PD, Fetz EE. Functional classes of primate corticomotoneuronal cells and their relation to act. *J Neurophysiol* 44: 773–791, 1980.

d'Avella A, Portone A, Fernandez L, Lacquaniti F. Control of fast-reaching movements by muscle synergy combinations. *J Neurosci* 26: 7791–7810, 2006.

Dayan P, Abbott LF. *Theoretical Neuroscience.* Cambridge, MA: The MIT Press, 2001.

Downloaded from jn.physiology.org on October 22, 2009

Devanne H, Cohen LG, Kouchtir-Devanne N, Capaday C. Integrated motor cortical control of task-related muscles during pointing in humans. *J Neurophysiol* 87: 3006–3017, 2002.

Ethier C, Brizzi L, Darling WG, Capaday C. Linear summation of cat motor cortex outputs. *J Neurosci* 26: 5574–5581, 2006a.

Ethier C, Charette G, Brizzi L, Roy F, Capaday C. The nature of the intrinsic connectivity of the cat motor cortex. *Soc Neurosci Abstr* 806.12, 2006b.

Gentner R, Classen J. Modular organization of finger movements by the human central nervous system. *Neuron* 52: 731–742, 2006.

Ghosh S, Fyffe RE, Porter R. Morphology of neurons in area 4 gamma of the cat's cortex studied with intracellular injection of HRP. *J Comp Neurol* 277: 290–312, 1988.

Gilbert CD. Adult cortical dynamics. *Physiol Rev* 78: 467–485, 1998.

Haider B, Duque A, Hasenstaub AR, McCormick DA. Neocortical network activity in vivo is generated through a dynamic balance of excitation and inhibition. *J Neurosci* 26: 4535–4545, 2006.

Huntley GW, Jones EG. Relationship of intrinsic connections to forelimb movement representations in monkey motor cortex: a correlative anatomic and physiological study. *J Neurophysiol* 66: 390–413, 1991.

Izzo PN. A note on the use of biocytin in anterograde tracing studies in the central nervous system: application at both light and electron microscopic level. *J Neurosci Methods* 36: 155–166, 1991.

Keller A. Intrinsic connections between representation zones in the cat motor cortex. *Neuroreport* 4: 515–518, 1993.

Keller A, Asanuma H. Synaptic relationships involving local axon collaterals of pyramidal neurons in the cat motor cortex. *J Comp Neurol* 336: 229–242, 1993.

Landry P, Labelle A, Deschenes M. Intracortical distribution of axonal collaterals of pyramidal tract cells in the cat motor cortex. *Brain Res* 191: 327–336, 1980.

Lamarre Y, Bioulac, B, Jacks. Activity of precentral neurons in conscious monkeys: effects of different. *J Physiol* 74: 253–264, 1978.

Lund JS, Yoshioka T, Levitt JB. Comparison of intrinsic connectivity in different areas of macaque monkey cerebral cortex. *Cereb Cortex* 3: 148–162, 1993.

McKiernan BJ, Marcario JK, Karrer JH, Cheney PD. Corticomotoneuronal postspike effects in shoulder, elbow, wrist, digit, and intrinsic hand muscles during a reach and prehension task. *J Neurophysiol* 80: 1961–1980, 1998.

Monfils MH, Plautz EJ, Kleim JA. In search of the motor engram: motor map plasticity as a mechanism for encoding motor experience. *Neuroscientist* 11: 471–483, 2005.

Rockland KS, Lund JS. Widespread periodic intrinsic connections in the tree shrew visual cortex. *Science* 215: 1532–1534, 1982.

Sanes JN, Schieber MH. Orderly somatotopy in primary motor cortex: does it exist? *Neuroimage* 13: 968–974, 2001.

Schieber MH. Rethinking the motor cortex. *Neurology* 52: 445–446, 1999.

Schneider C, Devanne H, Lavoie BA, Capaday C. Neural mechanisms involved in the functional linking of motor cortical points. *Exp Brain Res* 146: 86–94, 2002.

Schneider C, Zytnicki D, Capaday C. Quantitative evidence for multiple widespread representations of individual muscles in the cat motor cortex. *Neurosci Lett* 310: 183–187, 2001.

Shinoda Y, Arnold AP, Asanuma H. Spinal branching of corticospinal axons in the cat. *Exp Brain Res* 26: 215–234, 1976.

Sik A, Penttonen M, Ylinen A, Buzsaki G. Hippocampal CA1 interneurons: an in vivo intracellular labeling study. *J Neurosci* 15: 6651–6665, 1995.

Sik A, Tamamaki N, Freund TF. Complete axon arborization of a single CA3 pyramidal cell in the rat hippocampus, and its relationship with postsynaptic parvalbumin-containing interneurons. *Eur J Neurosci* 5: 1719–1728, 1993.

Tantisira B, Alstermark B, Isa T, Kummel H, Pinter M. Motoneuronal projection pattern of single C3-C4 propriospinal neurones. *Can J Physiol Pharmacol* 74: 518–530, 1996.

van Vreeswijk C, Sompolinsky H. Chaos in neuronal networks with balanced excitatory and inhibitory activity. *Science* 274: 1724–1726, 1996.

Van Hooser SD, Heimel JA, Chung S, Nelson SB. Lack of patchy horizontal connectivity in primary visual cortex of a mammal without orientation maps. *J Neurosci* 26: 7680–7692, 2006.

White EL. *Cortical Circuits.* Birkhauser, Basel, 1989.

Downloaded from jn.physiology.org on October 22, 2009